Load-Aware Stochastic Degradation Modeling and Lifetime Characterization for PEM Fuel Cells

Mouhamad Houjayrie[1], Catherine Cadet[1], and Christophe Bérenguer[1]

[1] *Université Grenoble Alpes, CNRS, Grenoble INP, GIPSA-lab, 38000 Grenoble, France*
mouhamad.houjayrie@grenoble-inp.fr
catherine.cadet@grenoble-inp.fr
christophe.berenguer@grenoble-inp.fr

ABSTRACT

The degradation of proton exchange membrane fuel cells (PEMFCs) is strongly dependent on load history and presents significant variability across nominally identical stacks. This paper proposes a physics-based, load-aware stochastic degradation framework for PEMFCs, with the objective of characterizing lifetime under static and dynamic operating profiles and providing a modeling basis for future Prognostics and Health Management (PHM) applications.

The cell voltage is described through a polarization model parameterized by degradation-sensitive quantities, namely the normalized electrochemically active surface area (ECSA), the membrane ohmic resistance, and the hydrogen crossover current. Catalyst degradation is represented by a simplified ECSA state driven by platinum dissolution–oxidation kinetics, while membrane ageing is described through a stochastic cumulative damage state modeled as a non-homogeneous Gamma process whose mean evolution is matched to a semi-empirical membrane degradation law. Membrane thickness and conductivity are reconstructed consistently from this damage state, and the resulting ohmic resistance and crossover current are fed back into the voltage model. Load dependence is enforced through the coupling between mission demand, operating-point computation, and voltage-driven degradation dynamics.

The resulting framework captures both intra-stack stochasticity, through the membrane damage process, and inter-stack variability, through dispersion in selected model parameters. A Health Index (HI) is defined as the normalized virtual rated-point voltage. Simulation studies under static and dynamic load profiles illustrate the influence of load level, load cycling, and parameter variability on degradation trajectories and lifetime distributions. Although state estimation and remaining useful life prediction are not addressed here, the proposed framework is intended to serve as a compact modeling basis for such future PHM developments.

1. INTRODUCTION

Proton exchange membrane fuel cells (PEMFCs) are widely regarded as a promising technology for low-emission energy conversion in transportation and stationary applications because of their high efficiency, low operating temperature, and rapid power response. Their large-scale deployment, however, remains limited by durability issues. In practice, fuel-cell performance progressively declines under operation, which reduces efficiency and shortens lifetime. These limitations motivate the development of Prognostics and Health Management (PHM) tools, which can support durability-oriented supervision.

Among the different components of a PEMFC, two of the main sources of long-term degradation are the catalyst layer and the proton exchange membrane. Catalyst degradation leads in particular to electrochemically active surface area (ECSA) loss, while membrane degradation induces thickness loss, conductivity decay, ohmic-resistance increase, and hydrogen crossover rise. A major difficulty is that these degradation mechanisms are strongly affected by the operating load. Extreme operating conditions, prolonged high-potential exposure, and repeated load variations can significantly accelerate degradation. Therefore, PEMFC lifetime cannot be viewed as an intrinsic quantity; it depends on the past and future operating profile. Another important feature is that PEMFC lifetime also shows randomness, so that even nominally identical stacks operated under similar conditions may show different degradation trajectories and different end-of-life times. A relevant durability model should therefore capture both the load dependence of degradation and its stochastic nature.

Several studies have addressed parts of this challenge. On one hand, a large number of works have focused on degradation

estimation and prediction using data-driven, model-based, or hybrid tools. For instance, hybrid prognostic schemes have combined polarization-based parameter extraction with learning models under dynamic operation (Yue, Li, Roche, Jemei, & Zerhouni, 2022), while observer-based approaches have estimated ageing-related parameters from voltage measurements for subsequent prediction (Ma, Xie, Xu, Huangfu, & Li, 2021). On the other hand, a smaller set of works has explicitly incorporated the effect of load into degradation modeling. A power-dependent lifetime model was proposed in which power decay is linked to experimentally identified stressor contributions such as high-load operation, idling, start–stop events, and load changes (Pei, Chang, & Tang, 2008). More recently, load-dependent stochastic deterioration models have been introduced for fuel cells by linking the degradation rate to load through empirical laws, for example through parabolic load–degradation-rate relations in Gamma-process formulations (Zuo, Cadet, Li, Bérenguer, & Outbib, 2024; Houjayrie, Cadet, & Bérenguer, 2025). In parallel, stochastic-process formulations based on Wiener dynamics have also been proposed, where a polarization-related parameter is modeled as a random process and then estimated or forecast using filtering and learning tools (Y. Hu, Zhang, Jiang, Peng, & Jin, 2023). These contributions clearly show the importance of both load dependence and stochasticity. However, the explicit link between operating load and degradation remains under-addressed at the level of physically interpretable internal degradation states.

This paper develops a load-aware stochastic degradation framework for PEMFCs in which the internal ageing mechanisms remain physically interpretable while uncertainty is introduced directly at the degradation-state level. The proposed model combines a simplified catalyst submodel for ECSA loss with a stochastic membrane-damage formulation based on a non-homogeneous Gamma process whose mean evolution is matched to a semi-empirical membrane degradation law. The resulting membrane damage is mapped consistently to thickness loss, conductivity decay, ohmic-resistance increase, and hydrogen crossover. These degradation states are then coupled to a polarization-based voltage model, from which a virtual rated-point HI is defined for lifetime characterization. To account for realistic operating conditions, the framework also includes a power–voltage coupling that links mission demand to the operating point and therefore to the degradation dynamics. Inter-stack variability is represented through dispersion in selected catalyst and membrane parameters.

The main contributions of this work are:

- a stochastic membrane degradation formulation based on a non-homogeneous Gamma process whose shape rate is linked to a semi-empirical membrane degradation law, yielding a consistent evolution of membrane thickness, conductivity, ohmic resistance, and hydrogen crossover current;
- a simplified catalyst-layer degradation model describing the evolution of the electrochemically active surface area (ECSA) through load-dependent platinum dissolution–oxidation kinetics, while remaining computationally efficient for long-term degradation simulations;
- a coupling between load demand and voltage-driven degradation, together with a simulation-based analysis of the impact of load history and parameter variability on degradation trajectories and resulting lifetime distributions.

2. VOLTAGE MODEL AND DEGRADATION-SENSITIVE QUANTITIES

We first introduce the polarization-based cell voltage model, since it describes how degradation affects performance and identifies the physical quantities involved in the degradation dynamics.

2.1. Polarization-based Cell Voltage Model

The per-cell terminal voltage is modeled in the usual form (Y. Wang, Moura, Advani, & Prasad, 2019):

$$U = E_{\mathrm{rev}} - \eta_{\mathrm{act}} - \eta_{\mathrm{ohm}} - \eta_{\mathrm{conc}}, \tag{1}$$

where E_{rev} is the reversible voltage and η_{act}, η_{ohm}, and η_{conc} are the activation, ohmic, and mass-transport overpotentials.

A Nernst-type expression adapted from (D. Hu, Wang, Li, Yang, & Wang, 2021) is used for the reversible voltage:

$$\begin{aligned} E_{\mathrm{rev}} = {} & 1.229 - 8.45 \times 10^{-4}(T - 298.15) \\ & + 4.31 \times 10^{-5}\, T \ln\!\left(p_{\mathrm{H_2}} \sqrt{p_{\mathrm{O_2}}}\right). \end{aligned} \tag{2}$$

where T is the cell temperature (K), and $p_{\mathrm{H_2}}$ and $p_{\mathrm{O_2}}$ are the hydrogen and oxygen partial pressures (bar).

Activation losses at the cathode follow a Tafel-type relation:

$$\eta_{\mathrm{act}} = \frac{RT}{\alpha_{\mathrm{ca}} F} \ln\!\left(\frac{j + i_{\mathrm{cross}}}{i_0}\right), \tag{3}$$

where j is the current density (A/cm^2), i_{cross} is the hydrogen crossover current density, α_{ca} is the cathodic transfer coefficient, R is the universal gas constant, and F is Faraday's constant.

The exchange current density depends on the catalyst state through the normalized ECSA S:

$$i_0(S, T, p_{\mathrm{O_2}}) = i_{0,\mathrm{ref}}\, S \left(\frac{p_{\mathrm{O_2}}}{p_0}\right)^{\gamma_{\mathrm{PO_2}}} \exp\!\left[-\frac{E_{\mathrm{ca}}}{R}\left(\frac{1}{T} - \frac{1}{T_0}\right)\right], \tag{4}$$

where $i_{0,\mathrm{ref}}$ is a reference exchange current density, p_0 is a

reference pressure, E_{ca} is an activation energy, and $\gamma_{\mathrm{PO_2}}$ is an oxygen-order exponent.

Ohmic losses are modeled as

$$\eta_{\mathrm{ohm}} = j\, R_{\mathrm{ohm}}, \tag{5}$$

where R_{ohm} is the membrane-related area-specific resistance.

Mass-transport losses are described by

$$\eta_{\mathrm{conc}} = -b_e \frac{RT}{4F} \ln\!\left(1 - \frac{j}{j_{\mathrm{lim}}(S)}\right), \tag{6}$$

where b_e is an empirical coefficient and the limiting current density depends on the catalyst state as (Y. Wang et al., 2019)

$$j_{\mathrm{lim}}(S) = \left(\frac{\frac{C_1}{A^0_{\mathrm{Pt}}} + C_2 + R_{\mathrm{O_2,DM}}}{\frac{C_1}{SA^0_{\mathrm{Pt}}} + C_2 + R_{\mathrm{O_2,DM}}}\right) j^0_{\mathrm{lim}}. \tag{7}$$

Here A^0_{Pt} is the initial Pt area per geometric area, j^0_{lim} is the initial limiting current density, and C_1, C_2, $R_{\mathrm{O_2,DM}}$ are oxygen-transport coefficients.

2.2. Degradation-Sensitive Quantities and State Definition

Eqs. (3)–(7) show that the cell voltage is directly affected by three degradation-sensitive quantities:

- the normalized electrochemically active surface area $S(t)$, which affects both the exchange current density i_0 and the limiting current density j_{lim};
- the membrane ohmic resistance $R_{\mathrm{ohm}}(t)$, which determines ohmic losses;
- the hydrogen crossover current density $i_{\mathrm{cross}}(t)$, which affects the activation losses and reflects the loss of membrane integrity.

These performance-sensitive quantities are derived from physically meaningful states:

$$x_{\mathrm{deg}}(t) = \big[S(t),\, L_{\mathrm{mem}}(t),\, \sigma_{\mathrm{mem}}(t)\big]^\top, \tag{8}$$

where $S(t)$ is the normalized ECSA, $L_{\mathrm{mem}}(t)$ the membrane thickness, and $\sigma_{\mathrm{mem}}(t)$ the membrane proton conductivity.

From these states, one obtains (Schoemaker, Misz, Beckhaus, & Heinzel, 2014):

$$R_{\mathrm{ohm}}(t) = \frac{L_{\mathrm{mem}}(t)}{\sigma_{\mathrm{mem}}(t)}, \qquad i_{\mathrm{cross}}(t) = \frac{p_{\mathrm{H_2}}(t)\,\psi_{\mathrm{H_2}}}{L_{\mathrm{mem}}(t)}\, 2F, \tag{9}$$

where $p_{\mathrm{H_2}}(t)$ is the hydrogen partial pressure and $\psi_{\mathrm{H_2}}$ is an effective hydrogen permeation coefficient.

The voltage can therefore be written compactly as

$$U(t) = U\big(j(t), x_{\mathrm{deg}}(t), u(t)\big), \tag{10}$$

where

$$u(t) = \big[T(t),\, p_{\mathrm{H_2}}(t),\, p_{\mathrm{O_2}}(t),\, RH(t)\big]^\top \tag{11}$$

collects the operating conditions, namely temperature, gas partial pressures, and relative humidity. The role of the degradation model is thus to propagate $x_{\mathrm{deg}}(t)$ under the applied load and operating conditions, after which voltage and performance degradation follow directly from the polarization relation.

3. LOAD-DEPENDENT STOCHASTIC DEGRADATION MODELING

We first model the membrane-related states through a stochastic Gamma process, then the catalyst state through a simplified ECSA model.

3.1. Stochastic Membrane Degradation Model

Membrane degradation is represented through a cumulative membrane-damage state, from which the membrane thickness $L_{\mathrm{mem}}(t)$ and proton conductivity $\sigma_{\mathrm{mem}}(t)$ are reconstructed. Since membrane damage is cumulative and non-decreasing, a Gamma process is a natural choice for modeling its evolution. It provides positive random increments and is therefore well suited to represent progressive irreversible damage accumulation (van Noortwijk, 2009).

We introduce a dimensionless cumulative membrane-damage state $Z_{\mathrm{mem}}(t)$, with

$$Z_{\mathrm{mem}}(0) = 0, \qquad Z_{\mathrm{mem}}(t) \geq 0, \tag{12}$$

and reconstruct the membrane thickness as

$$L_{\mathrm{mem}}(t) = L^0_{\mathrm{mem}}\big(1 - Z_{\mathrm{mem}}(t)\big), \tag{13}$$

where L^0_{mem} denotes the beginning-of-life membrane thickness. Thus, $Z_{\mathrm{mem}}(t)$ directly represents the cumulative fractional membrane-thickness loss.

The membrane proton conductivity is reconstructed from the same damage state as

$$\sigma_{\mathrm{mem}}(t) = \sigma^0_{\mathrm{mem}}\big(1 - K_\sigma Z_{\mathrm{mem}}(t)\big), \tag{14}$$

where σ^0_{mem} denotes the beginning-of-life conductivity. This relation assumes that conductivity decays proportionally to the cumulative membrane damage associated with thickness loss, with $K_\sigma > 0$ acting as the corresponding proportionality coefficient. With this definition, the same cumulative-damage state consistently drives both thickness loss and conductivity decay.

The linear reconstructions in Eqs. (13) and (14) are used only

within the physically admissible domain

$$0 \le Z_{\mathrm{mem}}(t) < Z_{\max}, \qquad Z_{\max} = \min\left(1, \frac{1}{K_\sigma}\right).$$

In the present lifetime simulations, the trajectories are propagated only up to the first passage of the end-of-life (EOL) threshold. Therefore, the model is not intended to describe post-EOL membrane collapse.

The membrane-damage increments are thus modeled as a non-homogeneous Gamma process:

$$Z_{\mathrm{mem}}(t+\Delta t) - Z_{\mathrm{mem}}(t) \sim \Gamma\big(\alpha_Z(t)\Delta t, \beta_{\mathrm{mem}}\big), \quad (15)$$

where $\Gamma(\alpha, \beta)$ denotes a Gamma distribution with shape parameter α and scale parameter β. Here, $\beta_{\mathrm{mem}} > 0$ is the Gamma-process scale parameter. For a given stack, it is constant over time, while population-level variability in β_{mem} is introduced later in Section 4.1.

To link the stochastic damage process to the operating conditions and, through the voltage, to the load demand, we rely on a semi-empirical membrane degradation law from the literature (Karpenko-Jereb, Sternig, Fink, & Tatschl, 2016). In their deterministic formulation, the membrane thickness evolves as

$$L_{\mathrm{mem}}(t) = L^0_{\mathrm{mem}}\Big(1 - r^{(L)}_{\mathrm{ref}} Y_{\mathrm{mem}}(t)\Big), \quad (16)$$

where $Y_{\mathrm{mem}}(t)$ is a cumulative degradation variable defined by

$$Y_{\mathrm{mem}}(t) = \int_0^t \phi(\tau)\,\mathrm{d}\tau. \quad (17)$$

The local degradation intensity $\phi(t)$ depends on voltage, temperature, relative humidity, and the current membrane thickness through

$$\phi(t) = \frac{a_0 + a_1 T(t) + a_2 RH(t) + a_3/\ln(L_{\mathrm{mem}}(t))}{a_0 + a_1 T_{\mathrm{ref}} + a_2 RH_{\mathrm{ref}} + a_3/\ln(L^{\mathrm{ref}}_{\mathrm{mem}})} \times \big(1.12U(t) - 0.06\big), \quad (18)$$

where $(T_{\mathrm{ref}}, RH_{\mathrm{ref}}, L^{\mathrm{ref}}_{\mathrm{mem}})$ denotes the reference operating point used for normalization, and $a_0, \ldots, a_3$ are empirical coefficients. The factor $\big(1.12U(t) - 0.06\big)$ captures the strong acceleration of membrane degradation at high voltage.

Our objective is to define the Gamma-process parameters so that the stochastic damage model remains consistent, in the mean, with Eq. (16). In particular, the mean increment of the Gamma process in Eq. (15) is

$$\mathbb{E}[Z_{\mathrm{mem}}(t+\Delta t) - Z_{\mathrm{mem}}(t)] = \alpha_Z(t)\beta_{\mathrm{mem}}\Delta t.$$

Therefore, to recover the Karpenko-Jereb thickness law in the mean, we choose

$$\alpha_Z(t) = \frac{r^{(L)}_{\mathrm{ref}}\phi(t)}{\beta_{\mathrm{mem}}}, \quad (19)$$

which yields

$$\mathbb{E}[Z_{\mathrm{mem}}(t+\Delta t) - Z_{\mathrm{mem}}(t)] = r^{(L)}_{\mathrm{ref}}\phi(t)\,\Delta t, \quad (20)$$

and

$$\mathrm{Var}[Z_{\mathrm{mem}}(t+\Delta t) - Z_{\mathrm{mem}}(t)] = \beta_{\mathrm{mem}}\, r^{(L)}_{\mathrm{ref}}\phi(t)\,\Delta t. \quad (21)$$

Hence,

$$\mathbb{E}[Z_{\mathrm{mem}}(t)] = r^{(L)}_{\mathrm{ref}} Y_{\mathrm{mem}}(t),$$

which implies

$$\mathbb{E}[L_{\mathrm{mem}}(t)] = L^0_{\mathrm{mem}}\Big(1 - r^{(L)}_{\mathrm{ref}} Y_{\mathrm{mem}}(t)\Big).$$

Therefore, the stochastic membrane model matches the Karpenko-Jereb thickness law in the mean, while also ensuring non-negative and monotone cumulative damage trajectories.

If the deterministic conductivity evolution is written as

$$\sigma_{\mathrm{mem}}(t) = \sigma^0_{\mathrm{mem}}\Big(1 - r^{(\sigma)}_{\mathrm{ref}} Y_{\mathrm{mem}}(t)\Big),$$

then consistency in the mean is obtained by choosing

$$K_\sigma = \frac{r^{(\sigma)}_{\mathrm{ref}}}{r^{(L)}_{\mathrm{ref}}}.$$

With this choice,

$$\mathbb{E}[\sigma_{\mathrm{mem}}(t)] = \sigma^0_{\mathrm{mem}}\Big(1 - r^{(\sigma)}_{\mathrm{ref}} Y_{\mathrm{mem}}(t)\Big).$$

Figure 1 illustrates the membrane-only stochastic degradation trajectories obtained under two constant imposed voltages, $U = 0.9$ V and $U = 0.6$ V, with fixed Gamma-process scale parameter $\beta_{\mathrm{mem}} = 10$. The figure shows the consistent joint evolution of $L_{\mathrm{mem}}(t)$, $\sigma_{\mathrm{mem}}(t)$, $R_{\mathrm{ohm}}(t)$, and $i_{\mathrm{cross}}(t)$ when all four quantities are reconstructed from the same Gamma-process damage state $Z_{\mathrm{mem}}(t)$. The higher-voltage case produces systematically faster membrane degradation, with a stronger decrease in thickness and conductivity and a corresponding stronger increase in ohmic resistance and hydrogen crossover.

3.2. Catalyst-layer Degradation (ECSA)

Loss of electrochemically active surface area (ECSA) in the cathode catalyst layer is a major source of PEMFC performance decay because it directly reduces the number of active platinum sites available for the oxygen reduction reaction. As the ECSA decreases, the exchange current density decreases,

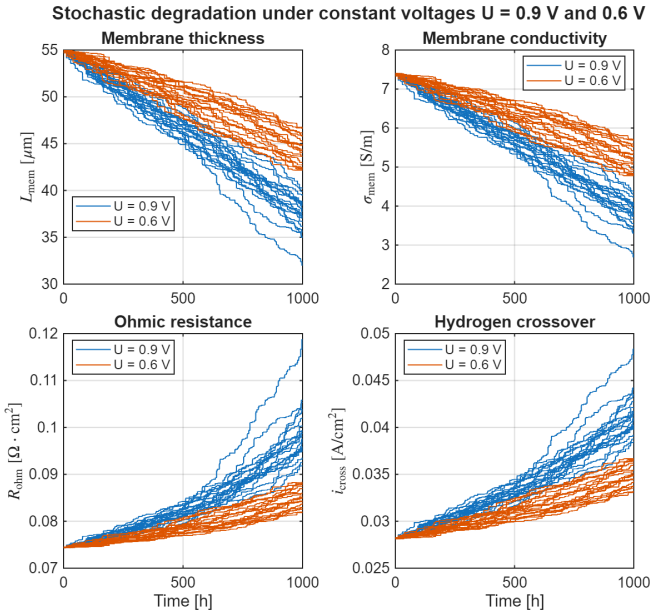

Figure 1. Membrane stochastic degradation trajectories under two constant imposed voltages, $U = 0.9$ V and $U = 0.6$ V, with fixed Gamma-process scale parameter $\beta_{\mathrm{mem}} = 10$. Each voltage case contains $N_{\mathrm{MC}} = 20$ stochastic trajectories and is used here as an illustrative membrane-only example.

activation losses increase, and the cell voltage deteriorates. In PEMFCs, this degradation is strongly potential-dependent and is therefore inherently load-driven.

At the mechanistic level, catalyst degradation is mainly governed by coupled platinum dissolution/redeposition and surface oxidation/reduction phenomena. At high cathode potentials, platinum becomes thermodynamically less stable and tends to dissolve, while the catalyst surface also becomes progressively covered by oxide species. When the potential is subsequently lowered, part of the dissolved platinum may redeposit and part of the oxide layer may be reduced. Repeated load variations therefore induce repeated oxidation/reduction cycles, whereas sustained high-voltage operation intensifies dissolution-driven loss of active surface area. In the present work, these mechanisms are represented through a simplified catalyst model derived from a more detailed multiscale Pt dissolution–oxidation formulation (Zhang & Pisu, 2014; Schneider, Sadeler, Scherzer, Zamel, & Gerteisen, 2019).

The catalyst state is described by two variables. The first one is the normalized ECSA,

$$S(t) = \frac{\mathrm{ECSA}(t)}{\mathrm{ECSA}(0)}, \qquad S(0) = 1, \tag{22}$$

which represents the remaining fraction of active catalyst surface. The second one is an averaged oxide-coverage state, denoted by $\theta_{\mathrm{ox}}(t)$, which represents the fraction of the platinum surface covered by oxide species. The corresponding simplified catalyst model is written as

$$\begin{aligned} \frac{\mathrm{d}S}{\mathrm{d}t} &= -k_A \exp\big(\gamma_U (U(t) - U_{\mathrm{ref}})\big)\big(1 - \theta_{\mathrm{ox}}(t)\big) S^3(t), \\ \frac{\mathrm{d}\theta_{\mathrm{ox}}}{\mathrm{d}t} &= \frac{1}{\tau_\theta}\big(\theta_{\mathrm{ox,ss}}(U(t)) - \theta_{\mathrm{ox}}(t)\big), \end{aligned} \tag{23}$$

with the steady-state oxide coverage

$$\theta_{\mathrm{ox,ss}}(U) = \frac{\theta_{\max}}{1 + \exp\big(-k_\theta (U - U_\theta)\big)}. \tag{24}$$

This formulation preserves the main physical trends of the underlying catalyst degradation mechanisms while remaining compact enough for long-term stochastic simulations. In Eq. (23), the parameter k_A acts as a coefficient controlling the overall degradation intensity. The exponential term introduces the strong sensitivity of Pt degradation to cathode potential, with γ_U controlling how sharply the degradation rate increases with voltage and U_{ref} serving as a reference potential for this acceleration. The factor $(1-\theta_{\mathrm{ox}})$ represents the oxide-free fraction of the platinum surface, so that oxide coverage directly affects the rate of dissolution/redeposition processes and hence S. The nonlinear term S^3 introduces a progressive slowing-down. In parallel, the oxide state $\theta_{\mathrm{ox}}(t)$ is modeled as a fast variable relaxing toward a voltage-dependent equilibrium. In Eq. (24), $\theta_{\max}$ denotes the saturation level of oxide coverage. The parameter τ_θ in Eq. (23) sets the time scale of the oxide dynamics.

The catalyst dynamics are described deterministically for a given parameter set. Nevertheless, the model also allows variability to be introduced through selected catalyst-related parameters, in particular the severity parameter k_A, in order to represent inter-stack differences in catalyst properties and degradation sensitivity. This aspect is not developed here, since the focus of this subsection is on the nominal load-dependent catalyst dynamics, but it is introduced later in Section 4.1.

The sensitivity of the simplified catalyst model to the operating load is illustrated in Figs. 2 and 3. Figure 2 shows the normalized ECSA under constant potential holds at 0.6, 0.8, and 0.9 V. After 500 h, the ECSA remains close to its initial value at 0.6 V (about 99%), decreases to roughly 74% at 0.8 V, and falls to about 49% at 0.9 V. This large spread confirms that even moderate increases in potential produce a much faster loss of active catalyst area. The curvature of the trajectories indicates that degradation is faster in the earlier phase and then progressively slows down.

Figure 3 shows the response under square-wave cycling between 0.6 and 0.95 V for two cycle periods. Although the voltage range is the same in both cases, the shorter period produces stronger degradation. After 500 h, the ECSA is approximately 41% for the 100 s cycle, compared with about

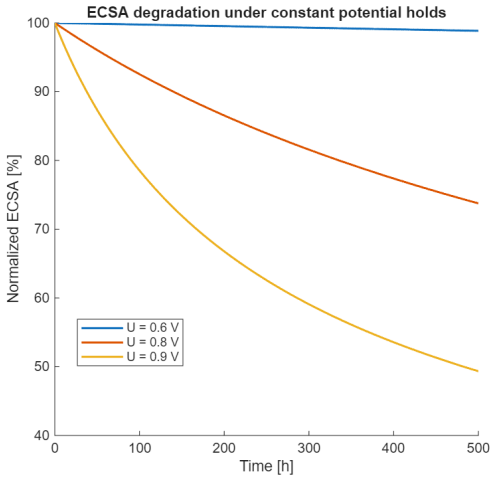

Figure 2. Normalized ECSA trajectories predicted by the simplified catalyst model under different constant potential holds. Higher voltage levels lead to significantly faster catalyst degradation.

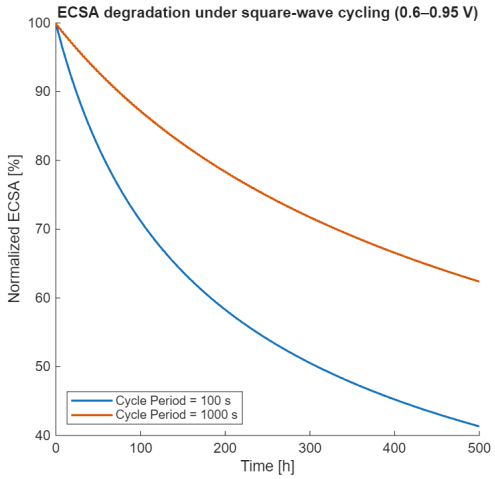

Figure 3. Normalized ECSA trajectories predicted by the simplified catalyst model under square-wave cycling between 0.6 and 0.95 V for different cycle periods. Faster cycling produces stronger catalyst degradation.

62% for the 1000 s cycle. The model is therefore sensitive not only to the load level but also to the temporal structure of the load. This behavior is physically consistent with the underlying mechanism: faster cycling induces more frequent oxidation/reduction transitions, which intensify catalyst stress and accelerate net ECSA loss.

The full derivation of this simplified catalyst model from the detailed multiscale formulation is not reported here because of space limitations. Instead, the simplified two-state model was calibrated against the full multiscale catalyst-layer model using constant-potential holds at 0.6, 0.8, and 0.9 V, and a square-wave profile between 0.6 and 0.9 V with a period of 6 s. Figure 4 compares the normalized ECSA trajectories predicted by the full and simplified models for these calibration protocols.

To complement this visual comparison, the approximation error was quantified over the 500 h horizon using samples every 300 s. The same calibrated parameters were also evaluated on additional voltage profiles that were not used during calibration. The resulting average errors are reported in Table 1. The simplified model achieves an average RMSE of 0.497 percentage points on the calibration profiles and 2.182 percentage points on the validation profiles, showing that it preserves the dominant ECSA degradation behavior of the detailed formulation while remaining compact for long-term simulations.

3.3. Health Index and End-of-Life

To compare degradation trajectories under different load histories, a scalar Health Index (HI) is defined at a fixed rated operating point. Let j_{rated} denote the rated current density,

Table 1. Average approximation error between the simplified and full ECSA models. Errors are expressed in percentage points (pp), except for the maximum relative error.

Set	RMSE [pp]	MAE [pp]	Max. err. [pp]	Max. rel. [%]
Calibration	0.497	0.414	1.132	2.28
Validation	2.182	2.059	3.381	6.21

and let

$$u_{\mathrm{rated}} := \left[T_{\mathrm{rated}},\, p_{\mathrm{H_2,rated}},\, p_{\mathrm{O_2,rated}},\, RH_{\mathrm{rated}}\right]^{\top} \tag{25}$$

denote the corresponding rated operating conditions. Given the degradation state

$$x_{\mathrm{deg}}(t) = \big(S(t), L_{\mathrm{mem}}(t), \sigma_{\mathrm{mem}}(t)\big)^{\top},$$

the virtual rated voltage is

$$U_{\mathrm{rated}}(t) = U\big(j_{\mathrm{rated}}, x_{\mathrm{deg}}(t), u_{\mathrm{rated}}\big), \tag{26}$$

and the beginning-of-life reference voltage is

$$U^{0}_{\mathrm{rated}} = U\big(j_{\mathrm{rated}}, x_{\mathrm{deg}}(0), u_{\mathrm{rated}}\big). \tag{27}$$

The HI is then defined as

$$\mathrm{HI}(t) = \frac{U_{\mathrm{rated}}(t)}{U^{0}_{\mathrm{rated}}}, \tag{28}$$

so that $\mathrm{HI}(0) = 1$ and $\mathrm{HI}(t)$ decreases as degradation progresses.

End-of-life (EOL) is defined by a threshold on this performance-based indicator:

$$\mathrm{HI}(t) \le \mathrm{HI}_{\mathrm{th}}, \qquad \mathrm{HI}_{\mathrm{th}} = 0.9, \tag{29}$$

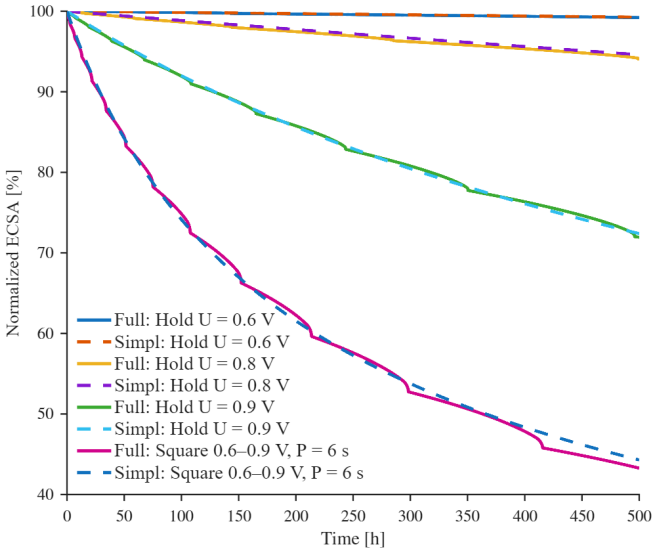

Figure 4. Comparison between the full multiscale catalyst-layer model and the simplified two-state ECSA model for the calibration voltage protocols.

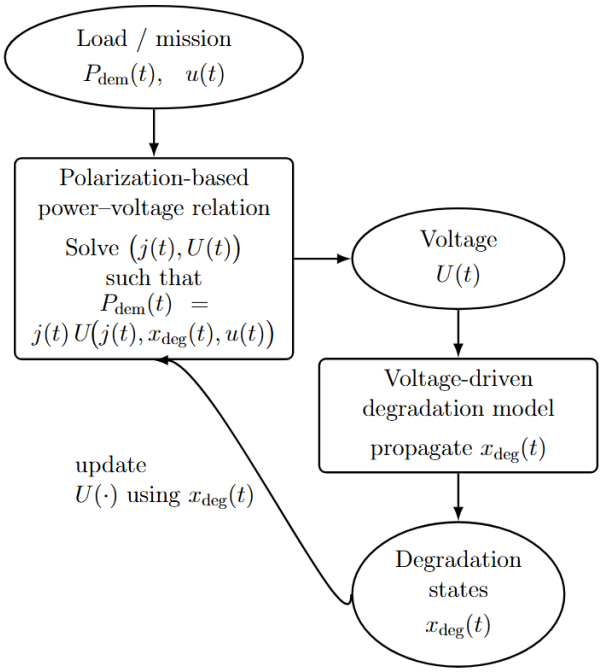

Figure 5. Modeling/simulation loop for load-dependent degradation. At each time step, the demanded specific power is coupled to the polarization model to determine the operating point, and the resulting voltage is used to update the degradation state, which then feeds back into the next operating-point computation.

which is consistent with the 10% rated-voltage-drop criterion commonly used in automotive PEMFC applications (Pei et al., 2008).

For a prescribed future load profile $j(\cdot)$, the mission-conditioned lifetime is the first-passage time to the threshold:

$$t_{\mathrm{EOL}} = \inf\big\{t \geq 0 : \mathrm{HI}(t) \leq \mathrm{HI}_{\mathrm{th}}\big\}. \tag{30}$$

This definition is used below to compare lifetime under different static and dynamic load scenarios.

3.4. Load-to-Voltage Coupling

The degradation laws used in this work are voltage-driven, whereas operation is more naturally specified in terms of load or demanded power. To enforce load dependence consistently, we couple the load demand to the polarization model and determine the operating point $(j(t), U(t))$ from the current degradation state.

Let $P_{\mathrm{dem}}(t)$ denote the demanded specific power, i.e., the demanded power normalized by active area. Given $P_{\mathrm{dem}}(t)$ and the current degradation state $x_{\mathrm{deg}}(t)$, the operating point $\big(j(t), U(t)\big)$ is obtained by solving

$$P_{\mathrm{dem}}(t) = j(t)\,U\big(j(t), x_{\mathrm{deg}}(t), u(t)\big), \tag{31}$$

with respect to the current density $j(t)$, after which $U(t)$ follows from Eq. (10). Over each short interval $[t, t+\Delta t]$, the degradation state is assumed constant while solving Eq. (31); the resulting voltage is then used to update the voltage-driven degradation laws over that interval. This updated degradation state then affects the next power–voltage relation, thereby closing the load–degradation loop shown in Fig. 5.

4. Lifetime Characterization Under Load and Parameter Variability

The previous sections define a stochastic, load-dependent degradation model for PEMFCs. We now use this framework to characterize degradation trajectories and lifetime under different load profiles. The goal is to study how operating history and parameter variability shape performance degradation and EOL. In the case studies below, the mission is described directly in terms of current-density profiles.

4.1. Inter-stack Variability Through Selected Model Parameters

The stochastic membrane model already captures intra-stack variability through the random Gamma-process increments. To represent inter-stack differences, selected model parameters are allowed to vary from one stack to another. Such variability may arise from differences in catalyst properties, membrane properties, fabrication conditions, or assembly-induced heterogeneity.

In the present paper, inter-stack variability is introduced through two parameters. First, the effective catalyst-severity parameter k_A, which enters the simplified ECSA law in Eq. (23), is allowed to vary across stacks. Physically, k_A represents an effective catalyst degradation-severity factor that

accounts for stack-specific catalyst characteristics, such as platinum loading and platinum particle-size distribution. In this work, k_A is modeled as a positive stack-specific random parameter following a lognormal distribution:

$$k_A^{(n)} \sim \text{Lognormal}(\mu_k, \sigma_k^2), \tag{32}$$

where μ_k and σ_k^2 are the log-scale mean and variance. Each stack therefore keeps its own fixed catalyst-severity parameter throughout its lifetime.

Second, inter-stack variability is also introduced in the membrane-damage model through the Gamma-process scale parameter. In practice, due to unobservable unit-specific effects, degradation trajectories may differ from one stack to another even under similar operating conditions. Such heterogeneity is commonly modeled in the literature by introducing random effects into Gamma-process degradation models, often through a unit-specific random scale parameter (X. Wang, Wang, Hong, & Jiang, 2021). In this work, the parameter β_{mem} is therefore treated as a positive stack-specific random effect and is modeled by a lognormal distribution:

$$\beta_{\text{mem}}^{(n)} \sim \text{Lognormal}(\mu_\beta, \sigma_\beta^2), \tag{33}$$

where μ_β and σ_β^2 are the corresponding log-scale parameters. In practice, $\beta_{\text{mem}}^{(n)}$ remains constant for a given stack over its lifetime, while varying across the population.

This allows the model to distinguish between within-stack randomness and between-stack heterogeneity while preserving the same physical degradation structure.

4.2. Monte Carlo Stochastic Lifetime Characterization

For a mission profile, expressed either directly as $j(t)$ or indirectly through $P_{\text{dem}}(t)$ and Eq. (31), the stochastic degradation model is simulated as follows:

1. for each stack $n = 1, \ldots, N_{\text{MC}}$, draw a catalyst-severity parameter $k_A^{(n)}$ from Eq. (32) and a membrane-dispersion parameter $\beta_{\text{mem}}^{(n)}$ from Eq. (33);
2. determine the operating point at each time step from the prescribed mission, either directly through the imposed current density or, when the mission is given in power form, by solving Eq. (31);
3. simulate the catalyst dynamics in Eq. (23) with $k_A = k_A^{(n)}$;
4. simulate the membrane-damage trajectory $Z_{\text{mem}}(t)$ using the non-homogeneous Gamma process in Eqs. (15)–(19) with $\beta_{\text{mem}} = \beta_{\text{mem}}^{(n)}$;
5. reconstruct $L_{\text{mem}}(t)$ and $\sigma_{\text{mem}}(t)$ through Eqs. (13)–(14), then compute $R_{\text{ohm}}(t)$ and $i_{\text{cross}}(t)$;
6. evaluate the HI through Eq. (28) and determine the EOL time by Eq. (30).

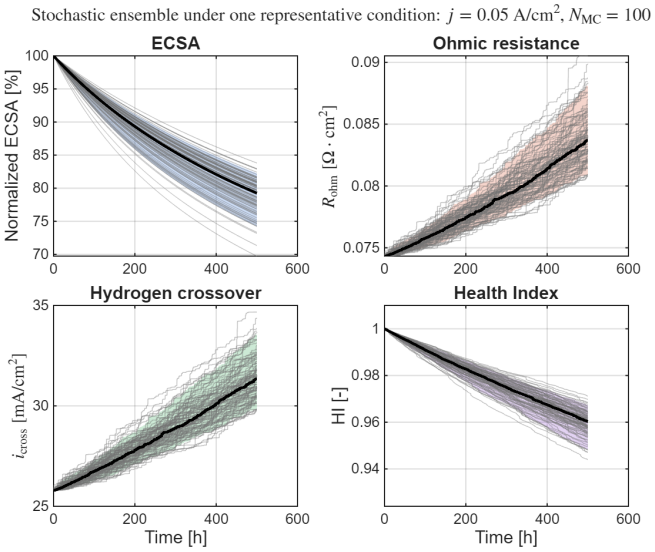

Figure 6. Illustrative ensemble of $N_{\text{MC}} = 100$ trajectory realizations obtained from the stochastic degradation model under one representative operating condition. The figure reports the normalized ECSA, ohmic resistance, hydrogen crossover current density, and Health Index. The individual trajectories are shown in gray, the median trajectory is shown by a thick black line, and the shaded region denotes the empirical 5–95% uncertainty band.

This procedure yields, for each stack, trajectory realizations of the degradation states, voltage, and HI, together with an associated EOL time, as illustrated in Fig. 6.

4.3. Load-dependent Lifetime Distributions

We now analyze the effect of load history directly through the stochastic degradation model by comparing the resulting lifetime distributions under several operating scenarios.

Five representative load cases are considered: two static operating points and three square-wave profiles. The static cases correspond to constant current densities of $j = 0.05\ \text{A/cm}^2$ (very low load, high-voltage operation) and $j = 0.8\ \text{A/cm}^2$ (higher load, moderate-voltage operation). The square-wave profiles alternate between low and high current levels with a 50% duty cycle: two large-amplitude profiles switching between $j_{\text{low}} = 0.05\ \text{A/cm}^2$ and $j_{\text{high}} = 0.8\ \text{A/cm}^2$ with periods $P = 1000$ s and $P = 100$ s, and a third fast profile in which the low-current level is raised to $j_{\text{low}} = 0.20\ \text{A/cm}^2$.

For each load case, $N_{\text{MC}} = 100$ trajectory realizations are simulated. This sample size was found sufficient, as increasing the number of realizations did not materially change the estimated lifetime distributions. EOL is defined as the first passage of the HI to $\text{HI}_{\text{th}} = 0.9$ at the rated current density. The lifetime distributions shown below are obtained from the resulting Monte Carlo EOL samples using kernel density estimation, rather than displayed as raw histograms. Since the

EOL distributions are not necessarily symmetric, the median and mean EOL values are reported together for each scenario.

The results show a clear influence of the load profile on the full lifetime distribution. The static low-load profile $j = 0.05\ \mathrm{A/cm^2}$ produces the shortest lifetimes, with a median/mean EOL of about $1098/1127$ h. This reflects the strong penalty associated with sustained operation at very low current and high voltage, which accelerates both catalyst and membrane degradation. Increasing the static load to $j = 0.8\ \mathrm{A/cm^2}$ shifts the distribution toward much longer lifetimes, with a median/mean EOL around $2103/2189$ h, indicating a substantially less aggressive operating regime.

The square-wave cases lie between these two static extremes. Large-amplitude switching between $(0.05 \leftrightarrow 0.8)\ \mathrm{A/cm^2}$ yields a median/mean EOL around $1395/1481$ h for the slow case ($P = 1000$ s), whereas the fast case ($P = 100$ s) yields a much shorter median/mean EOL of about $1115/1170$ h. The latter distribution lies very close to that of the static low-load case, showing that fast, deep load oscillations can nearly reproduce the same degradation severity as prolonged operation at very low load. Raising the low-current level to $0.20\ \mathrm{A/cm^2}$ in the fast square wave extends the median/mean EOL to about $1690/1761$ h, showing that reducing the depth of the load swing can significantly mitigate degradation even when the switching remains fast.

Overall, these results show that the load effect can be discussed directly at the stochastic level, since the proposed model simultaneously captures the operating-condition dependence of the degradation rate and the dispersion of trajectories around that mean behavior. In particular, the model reveals three coupled effects on lifetime: the average load level, the temporal structure of the mission, and the uncertainty propagated through the degradation states. Avoiding prolonged high-voltage operation and limiting both the depth and the frequency of load swings therefore emerge as key levers for extending lifetime.

The resulting EOL distributions for the five load scenarios are compared in Fig. 7. These kernel density estimates provide a compact and decision-relevant summary of how mission design influences both expected durability and uncertainty on lifetime.

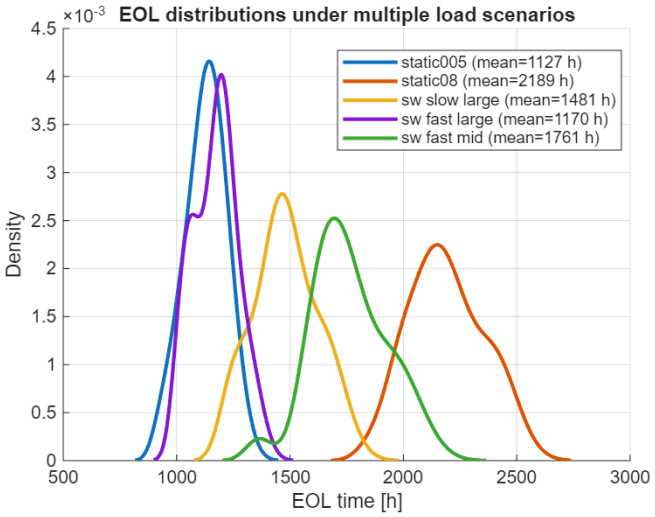

Figure 7. Kernel density estimates of EOL times under five representative load scenarios: two static operating points and three square-wave missions.

5. PHM RELEVANCE AND POSSIBLE EXTENSIONS

Although this paper focuses on the modeling and on lifetime characterization under prescribed load profiles, the proposed framework has been built with PHM-oriented applications in mind.

First, the degradation is expressed through physically interpretable states that directly drive voltage degradation. This makes the model suitable for future state-estimation schemes, since hidden degradation states such as $S(t)$ or membrane-related variables can in principle be inferred from voltage and operating data through observers or Bayesian filters. In the same spirit, some stack-specific degradation parameters, such as effective catalyst-severity or membrane-dispersion parameters, could also be identified individually for each stack by embedding the model into a filtering framework and estimating them jointly with the states from operational data.

Second, if sufficiently rich data become available at the population level, for example operating histories together with end-of-life observations for many stacks, the same modeling framework could be used in a statistical identification setting. In that case, the distributions of stack-specific parameters could be inferred from data rather than prescribed a priori, and the underlying modeling assumptions on inter-stack variability and intra-stack stochasticity could be assessed and refined accordingly.

Third, the stochastic membrane formulation makes the model naturally compatible with future remaining useful life (RUL) prediction methods. Once measurements become available and a state-estimation framework is added, the same model can be propagated forward under assumed future missions to generate conditional lifetime forecasts.

Finally, because the model remains compact while preserving explicit load dependence, it can serve as a per-stack building block for future health-aware energy management and maintenance strategies in multi-stack PEMFC systems.

6. CONCLUSION

The results show that PEMFC lifetime is strongly shaped by the operating profile, not only through the average load level but also through the temporal structure of the mission. In par-

ticular, prolonged low-load operation, which corresponds to sustained high-voltage conditions, leads to faster degradation and shorter lifetime, while frequent and deep load variations further accelerate ageing compared with smoother profiles.

At the catalyst level, the simplified ECSA model captures the strong sensitivity of platinum-surface degradation to both voltage level and load dynamics: higher operating potentials and faster cycling produce significantly stronger ECSA loss, although the ECSA degradation rate progressively slows down as the active surface decreases. At the membrane level, the stochastic damage formulation generates physically consistent trajectories of thickness loss, conductivity decay, ohmic-resistance increase, and hydrogen crossover rise, while naturally introducing dispersion in lifetime; in contrast to the catalyst behavior, membrane-related performance losses tend to accelerate as degradation progresses. This difference in temporal behavior between catalyst and membrane degradation may be particularly relevant for future ageing-mitigation strategies.

Taken together, these results make the framework relevant for future durability assessment, prognostics, and health-aware decision-making under realistic operating missions, including both energy-management and maintenance-oriented strategies.

ACKNOWLEDGMENT

This work was supported by the French National Research Agency (ANR) under the MFC-DEPLOY project, ANR-23-CE05-0006.

REFERENCES

Houjayrie, M., Cadet, C., & Bérenguer, C. (2025, June). Prognostic and Energy Management for Multi-Stack Fuel Cell Systems with Stochastic Non-Homogeneous Degradation. In E. B. Abrahamsen, T. Aven, F. Bouder, R. Flage, & M. Ylönen (Eds.), *Proceedings of the 35th European Safety and Reliability & the 33rd Society for Risk Analysis Europe Conference* (pp. 1530–1537). Stavanger, Norway: Research Publishing Singapore. Retrieved 2025-11-20, from https://hal.science/hal-05279594 (Backup Publisher: European Safety and Reliability Conference and Society of Risk Analysis - Europe) doi: 10.3850/978-981-94-3281-3_ESREL-SRA-E2025-P7472-cd

Hu, D., Wang, Y., Li, J., Yang, Q., & Wang, J. (2021, December). Investigation of optimal operating temperature for the PEMFC and its tracking control for energy saving in vehicle applications. *Energy Conversion and Management*, *249*, 114842. Retrieved 2025-05-21, from https://www.sciencedirect.com/science/article/pii/S0196890421010189 doi: 10.1016/j.enconman.2021.114842

Hu, Y., Zhang, L., Jiang, Y., Peng, K., & Jin, Z. (2023, April). A Hybrid Method for Performance Degradation Probability Prediction of Proton Exchange Membrane Fuel Cell. *Membranes*, *13*(4), 426. Retrieved 2026-03-08, from https://pmc.ncbi.nlm.nih.gov/articles/PMC10142057/ doi: 10.3390/membranes13040426

Karpenko-Jereb, L., Sternig, C., Fink, C., & Tatschl, R. (2016, August). Membrane degradation model for 3D CFD analysis of fuel cell performance as a function of time. *International Journal of Hydrogen Energy*, *41*(31), 13644–13656. Retrieved 2025-09-19, from https://www.sciencedirect.com/science/article/pii/S0360319916316512 doi: 10.1016/j.ijhydene.2016.05.229

Ma, R., Xie, R., Xu, L., Huangfu, Y., & Li, Y. (2021, December). A Hybrid Prognostic Method for PEMFC With Aging Parameter Prediction. *IEEE Transactions on Transportation Electrification*, *7*(4), 2318–2331. Retrieved 2025-05-15, from https://ieeexplore.ieee.org/document/9417096/ doi: 10.1109/TTE.2021.3075531

Pei, P., Chang, Q., & Tang, T. (2008, July). A quick evaluating method for automotive fuel cell lifetime. *International Journal of Hydrogen Energy*, *33*(14), 3829–3836. Retrieved 2025-09-17, from https://www.sciencedirect.com/science/article/pii/S036031990800476X doi: 10.1016/j.ijhydene.2008.04.048

Schneider, P., Sadeler, C., Scherzer, A.-C., Zamel, N., & Gerteisen, D. (2019, March). Fast and Reliable State-of-Health Model of a PEM Cathode Catalyst Layer. *Journal of The Electrochemical Society*, *166*(4), F322. Retrieved 2025-05-16, from https://iopscience.iop.org/article/10.1149/2.0881904jes/meta doi: 10.1149/2.0881904jes

Schoemaker, M., Misz, U., Beckhaus, P., & Heinzel, A. (2014, June). Evaluation of Hydrogen Crossover through Fuel Cell Membranes. *Fuel Cells*, *14*. doi: 10.1002/fuce.201300215

van Noortwijk, J. M. (2009). A survey of the application of gamma processes in maintenance. *Reliability Engineering and System Safety*, *94*(1), 2–21. Retrieved 2026-03-17, from https://ideas.repec.org//a/eee/reensy/v94y2009i1p2-21.html

Wang, X., Wang, B. X., Hong, Y., & Jiang, P. H. (2021, August). Degradation data analysis based on gamma process with random effects. *European Journal of Operational Research*, *292*(3), 1200–

1208. Retrieved 2026-03-17, from https://www.sciencedirect.com/science/article/pii/S0377221720309826 doi: 10.1016/j.ejor.2020.11.036

Wang, Y., Moura, S. J., Advani, S. G., & Prasad, A. K. (2019, March). Power management system for a fuel cell/battery hybrid vehicle incorporating fuel cell and battery degradation. *International Journal of Hydrogen Energy*, *44*(16), 8479–8492. Retrieved 2025-05-21, from https://www.sciencedirect.com/science/article/pii/S0360319919305014 doi: 10.1016/j.ijhydene.2019.02.003

Yue, M., Li, Z., Roche, R., Jemei, S., & Zerhouni, N. (2022, January). Degradation identification and prognostics of proton exchange membrane fuel cell under dynamic load. *Control Engineering Practice*, *118*, 104959. Retrieved 2025-05-15, from https://www.sciencedirect.com/science/article/pii/S0967066121002367 doi: 10.1016/j.conengprac.2021.104959

Zhang, X., & Pisu, P. (2014). Prognostic-oriented Fuel Cell Catalyst Aging Modeling and Its Application to Health-Monitoring and Prognostics of a PEM Fuel Cell. *International Journal of Prognostics and Health Management*, *5*(1). Retrieved 2024-11-25, from https://papers.phmsociety.org/index.php/ijphm/article/view/2203 (Number: 1) doi: 10.36001/ijphm.2014.v5i1.2203

Zuo, J., Cadet, C., Li, Z., Bérenguer, C., & Outbib, R. (2024, January). A deterioration-aware energy management strategy for the lifetime improvement of a multi-stack fuel cell system subject to a random dynamic load. *Reliability Engineering & System Safety*, *241*, 109660. Retrieved 2024-12-02, from https://www.sciencedirect.com/science/article/pii/S0951832023005744 doi: 10.1016/j.ress.2023.109660